A 0-D Electric Gun Model for the Optimization of Flyer Acceleration to Hypervelocities

Mila D. Fitzgerald, James D. Pecover, Nik Petrinic, and Daniel E. Eakins

***Abstract*— The electric gun is a pulsed power projectile launcher that utilizes the rapid expansion of an ohmically heated exploding foil and electromagnetic (EM) forces to accelerate thin flyers up to 20 km/s. Though the launcher has high energetic efficiencies when compared to alternative techniques, the process of launching flyers above 0.5 mm thickness in this manner often results in uncontrolled launch characteristics and premature failure of the flyer. This behavior is challenging to model numerically, limiting optimization work to sophisticated and computationally intensive magneto-hydrodynamics (MHD) codes. This work presents a 0-D model designed to expedite the parametric optimization process of electric gun loads to launch thick flyers to hypervelocities. The model is capable of predicting not only the foil state and flyer dynamics, but uses a novel approximation to predict the maximum pressure state in the flyer. The model is verified against 3-D MHD Eulerian hydrocode "Code 𝔹" and the validity of the approximations made in simplifying the model are discussed. With this model, the electric gun could be optimized to launch thicker flyers and achieve higher pressures and shock durations, enabling it to become a complimentary tool to existing projectile launch platforms.**

***Index Terms*— Electromagnetic (EM) accelerators, electrothermal launch, EM launch, pulsed power.**

I. Introduction

THE conditions experienced by spacecraft, lunar habitats, and fusion reactors, to name a few examples, are unlike any found naturally on the Earth's surface, reaching extreme pressures and temperatures during operation. Access to these conditions in a controlled setting enables the selection and design of resilient materials for these applications, which, in turn, relies on advancement of techniques to generate ever more extreme material states. The electric gun is one such technique; a pulsed power launcher which utilizes rapid discharge of a capacitor bank to accelerate a flyer to velocities up to 20 km/s. It is generally used in high pressure equation of state (EoS) research and hypervelocity ballistic testing. Much of the early activity on electric guns took place at Lawrence Livermore National Laboratory (LLNL), from 1976 to around 1990 [1], [2], [3]. More recently, the technique experienced a revival in laboratories in China [4], [5], [6].

The electric gun can be thought of as a hybrid between the exploding foil initiator (EFI), also known as a "slapper," and the electromagnetic (EM) plate flyer launcher [7], [8]. Its projectile is driven by both a thermal explosion, as in an EFI, and the magnetic acceleration of the plate flyer. The process begins with the discharge of a high-speed capacitor bank across a thin metallic foil, resulting in a large amount of energy deposited in the foil through ohmic heating. This energy deposition drives a change in the foil state from solid to a rapidly expanding plasma. The foil plasma acts as a driver gas, accelerating an adjacent thin plate, referred to as the "flyer." The flyer plate is laid atop the foil in a bonded stiff assembly, such that the foil plasma "punches out" a section of the flyer material, accelerating it typically for a few millimeters to impact a target. The plasma pressure component of the acceleration is known as the thermal drive. When large currents are discharged to vaporize the foil, considerable magnetic forces exist in the system that also act to accelerate the foil plasma. This effect is referred to as the magnetic drive.

The electric gun has demonstrated conversion from electrical capacitor bank discharge to projectile kinetic energy of up to around 15% [9]. The approach's high efficiencies emerge from its ability to convert energy from both the thermal explosion and the magnetic fields, inherent in the system, into kinetic energy in the flyer. The magnetic contribution to the acceleration allows far higher flyer velocities and impact pressures than can be achieved using an EFI, meanwhile, the addition of Joule heating to the work done accelerating the flyer gives the electric gun an energetic advantage over the EM plate flyer. Despite its higher efficiencies, the electric gun is not currently a viable alternative to the EM plate flyer due to constraints in the thickness of flyers it can successfully launch. Electric gun flyers thicker than 0.5 mm exhibit a violent change in state during launch and flight, often experiencing complete disintegration when using high energy capacitor banks [6]. The thin nature of the flyers launched induce strong but short duration shocks in targets, preventing the electric gun from investigating longer timescale phenomena and limiting its applications.

Adapting the design of the electric gun to launch thicker flyers relies on better understanding of the mechanisms responsible for flyer breakup at larger thicknesses. In situ collection of data regarding the operation of the electric gun

Manuscript received 13 June 2023; revised 7 July 2023; accepted 23 July 2023. The review of this article was arranged by Senior Editor R. P. Joshi. *(Corresponding author: Mila D. Fitzgerald.)*

Mila D. Fitzgerald is with the Department of Engineering Science, University of Oxford, OX1 2JD Oxford, U.K., and also with First Light Fusion, OX5 1QU Yarnton, U.K. (e-mail: mila.fitzgerald@outlook.com).

James D. Pecover is with First Light Fusion, OX5 1QU Yarnton, U.K.

Nik Petrinic and Daniel E. Eakins are with the Department of Engineering Science, University of Oxford, OX1 2JD Oxford, U.K.

Color versions of one or more figures in this article are available at https://doi.org/10.1109/TPS.2023.3300093.

Digital Object Identifier 10.1109/TPS.2023.3300093

during launch and flight prior to impact is challenging, time consuming, and resource-intensive. Instead, accurate modeling of the electric gun operating mechanism is a more efficient route to better understanding the interaction between the exploding foil plasma and flyer. Researchers initially struggled to numerically model the interplay between the thermal and magnetic components of acceleration in the electric gun, using simple empirical circuit models for the foil explosion [10] and the Gurney model to predict the final flyer velocity [1]. Though successful for smaller capacitor banks, these models failed to capture the behavior of flyers launched above 10 km/s, where magnetic forces become significant. To account for this effect, Osher et al. [3] and Lindemuth et al. [11] adapted Lindemuth's computational model for exploding metallic switches to create a version of the 1-D magnetohydrodynamics (MHD) code specific to the electric gun capable of modeling the dynamics and state of the exploding foil. However, the model does not consider the flyer state when calculating the flyer dynamics, making it only accurate when modeling launch of flyers under 0.5 mm thickness. Lack of consideration of the flyer state in Osher's model extends into other electric gun models, preventing simple models from being used to investigate the launch thicker of flyers [5], [12].

As simplified models for the electric gun have no means of calculating flyer state, parametric studies for numerical optimization of the electric gun load rely upon sophisticated hydrocodes, able to model both MHD and material EoS in the foil and flyer. Not only is access to these codes limited, but the complexity of the electric gun and corresponding multiphysics requires expensive computational resource. When compared to well understood launch platforms such as gas guns, or EM launchers which can rely on established simplified modeling techniques for optimization, [13] it is understandable why the electric gun is not used more broadly. However, if a more accessible code capable of modeling the electric gun flyer state was made available, the projectile launcher could be more readily optimized to launch thick flyers on a range of pulsed power devices, enabling existing launch platforms to access the full potential of this research tool.

In this work, a model was developed for the purpose of understanding the pressure state in the flyer during launch and flight. Unlike previous 0-D models used to investigate EM and thermal launch of projectiles, this model is capable of predicting states in both the foil and the flyer as well as the flyer dynamics, using a novel technique to approximate the pressure at the foil-flyer interface. This capability allows the user to perform large scale parameter scans which can consider maximum flyer pressure in minutes, as opposed to days in an MHD hydrocode with access to high performance computing. This both expedites the optimization process of an electric gun set-up, and allows those without access to an advanced multiphysics hydrocode to design an electric gun for a specific pulsed power machine. Using the 0-D model in parallel with a 3-D MHD hydrocode to perform verification, this work investigates the following questions.

1) Can modeling of the flyer state during electric gun operation be achieved based on prior understanding of phenomena in EM launchers?
2) How does the interplay between EM, thermal and hydrodynamic behavior influence the pressure states in the foil and flyer?
3) Which effects in electric gun operation contribute most significantly to the flyer state?
4) Over what range is the presented model valid, and why is this the case?

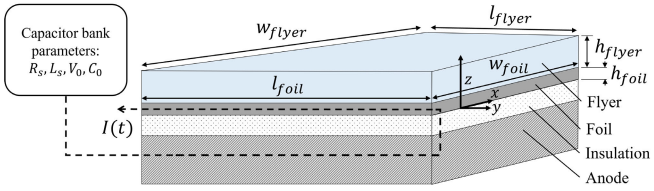

Fig. 1. 0-D model allows the user to input detailed parameters regarding the foil, flyer and capacitor bank. These include the foil and flyer material and dimensions, and the capacitor bank parameters necessary for calculating the system current at each timestep.

II. 0-D Model: Algorithm and Physics

The electric gun model presented in this work represents the electric gun load as an RLC circuit to determine the current through the metal foil in the electric gun in 0-D. 0-D simulation refers to a model where physical behavior is treated without spatial dependency but with time dependency, with the effect of reducing the computational complexity of the problem. Fig. 1 presents the range of parameters for input geometries of the foil and flyer and machine parameters, which allow the model to calculate results for specific load designs.

The model algorithm can be broken into four sections. First, the current is calculated in each timestep (Section II-A). This is then used to find the change in the state in the foil, and update three positions in the electric gun system; the rear of the foil, the interface between the foil and flyer, and the front of the flyer (Section II-B). Next, using both the foil state and positions, a pressure gradient from the maximum pressure in the foil to the front of the flyer is established (Section II-C). Finally, by using the position of the magnetic field along the z-axis to find the location of the maximum pressure in the foil, the pressure at the foil-flyer interface, assumed to be the maximum pressure in the flyer, is calculated (Section II-D). This section will explore the details of the steps in the order of the algorithm, which is visualized in Fig. 2.

A. Electric Gun RLC Circuit Model

The electric gun load operates by discharging a large current produced by a pulsed power generator to a metallic foil. This circuit can be represented by the RLC circuit equations, which may be represented as

$$\frac{dI}{dt} = \frac{1}{L(t)}\left[V(t) - I(t)\left(R(t) + \frac{dL}{dt}\right)\right] \tag{1a}$$

$$L = L_s + L_{\text{foil}} \tag{1b}$$

$$R = R_s + R_{\text{foil}} \tag{1c}$$

where I is the current, $V(t)$ is the voltage, L and R are the total system inductance and resistance, comprised of

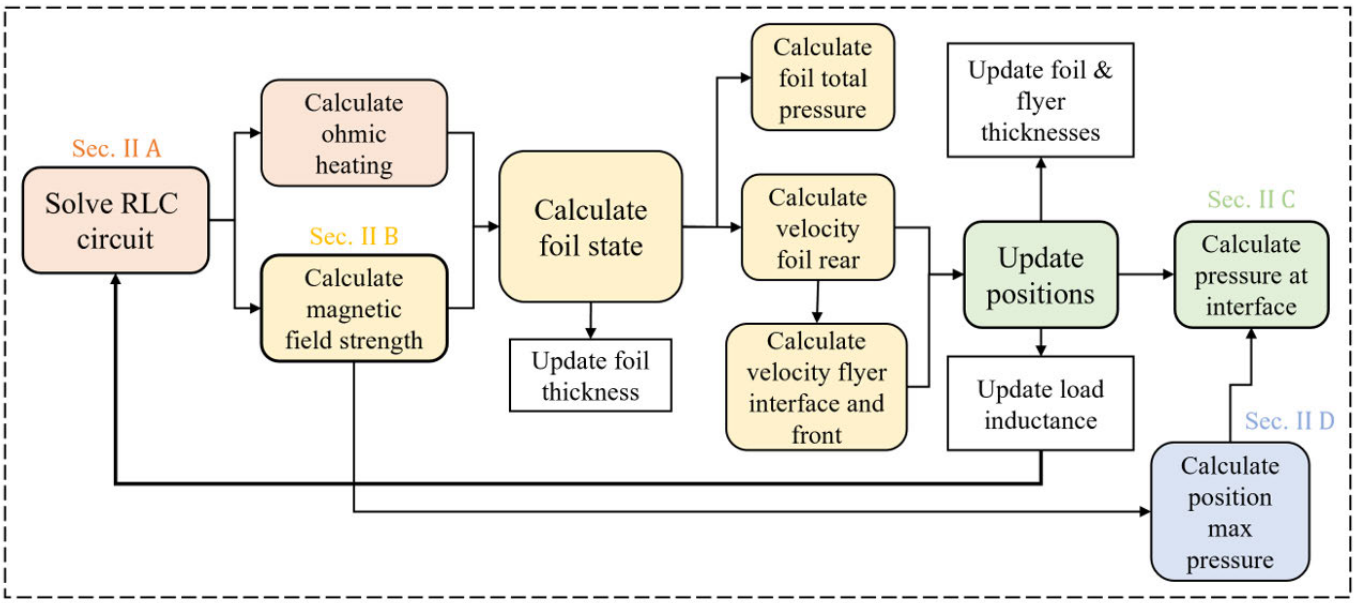

Fig. 2. Flowchart demonstrates the model algorithm characterized as four stages Section II-A calculation of the current in the RLC circuit, Section II-B calculation of the foil state, Section II-C updates positions and pressure gradient, and Section II-D gives the calculation of the pressure in the flyer. The flowchart also illustrates the dependencies of the calculated values on those upstream; clearly if the pressure in the flyer is to be calculated accurately, the foil state and projectile dynamics must be also.

L_s and R_s, the fixed machine inductance and resistance, and L_{foil} and R_{foil}, the time dependent load inductance and resistance, respectively.

The discharging circuit can be expressed as

$$V(t) = -V_c = -\frac{Q(t)}{C(t)} \tag{2}$$

where V_c is the charge voltage and $Q(t)$ are the machine charge and $C(t)$ is the capacitance as the machine discharges. The circuit equation can be solved using the explicit Euler method by assuming a constant capacitance C_0, such that

$$\frac{dV}{dt} = -\frac{I(t)}{C_0}. \tag{3}$$

The foil's inductance, and thus the current, are dependent on the conductor's flight position (z). The axes and origin for this problem is shown in Fig. 3. The model utilizes an inductance equation developed by Novac et al. [13] specific to plate flyers, which states

$$L_d(z) = \begin{cases} \dfrac{\mu_0 l_{\text{foil}}}{\pi} \ln\left(\dfrac{8x^2 + w_{\text{foil}}^2}{2w_{\text{foil}} z}\right), & \text{for } z > 2w_{\text{foil}} \\ \dfrac{\mu_0 l_{\text{foil}}}{\frac{w_{\text{foil}}}{z} + 1.21 - 0.11\frac{z}{w_{\text{foil}}} + \left(1 - \frac{z}{2w_{\text{foil}}}\right)^6}, & \text{otherwise} \end{cases} \tag{4}$$

where μ_0 is the vacuum permeability, l_{foil} is the foil length, w_{foil} is the foil width, and z is the flight direction. The foil inductance in time is then found using the velocity, $v_z(t)$, at each timestep

$$\frac{\partial L}{\partial t} = \frac{\partial z}{\partial t}\frac{\partial L}{\partial z} = v_z(t)\frac{\partial L}{\partial z} \tag{5}$$

allowing the circuit to take both the position and velocity of the foil into account as time progresses.

The foil resistance may be approximated as

$$R_{\text{foil}}(t) = \frac{l}{w}\eta(t) \tag{6}$$

where the resistivity $\eta(t)$ is calculated using the Burgess model [14], which is both temperature and state dependent. To calculate the change in temperature in the foil, the heating power Q_h can be calculated using

$$Q_h = \int_0^t I(t)^2 R_{\text{foil}}\, dt \tag{7}$$

with the subsequent temperature change in the foil approximated from solid state through to vapor using the change in energy in the foil

$$E_1 = \Delta E_{\text{heat solid}} = c_s M(T_m - T_0) \tag{8a}$$
$$E_2 = E_1 + \Delta E_m = E_1 + H_m M \tag{8b}$$
$$E_3 = E_2 + \Delta E_{\text{heat liquid}} = E_2 + c_L M(T_v - T_m) \tag{8c}$$
$$E_b = E_3 + \Delta E_v = E_3 + H_v M. \tag{8d}$$

Here, c_s refers to the solid heat capacity, M refers to the foil mass, T_m is the melting temperature of the foil, T_0 is the initial temperature of the foil, H_m is the heat of fusion, c_L is the liquid heat capacity, T_v is the boiling temperature, and H_v is the heat of vaporization.

R_{foil} is updated each timestep so the model can account for the complex change in resistivity as the foil transitions from solid to plasma.

B. EM and Thermal Acceleration

The flyer in the electric gun is subject to forces due to both the EM field and the expanding foil plasma. The following

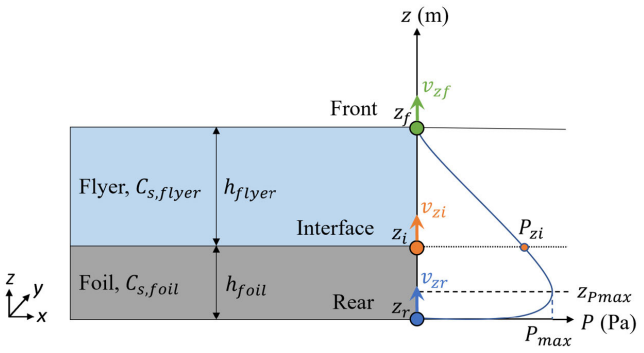

Fig. 3. Positions of the four locations used determine the pressure at the foil-flyer interface, alongside the velocities used to approximate the foil-flyer dynamics. An example of a realistic plot of pressure in the foil and flyer is included. The model assumes the foil and flyer form a continuous interface, the pressure at the front of the flyer is zero and the pressure gradient between z_{Pmax} and z_f is linear.

approach to finding the accelerating force (F_z) was derived by Novac et al. [13]. To calculate the EM force applied to the flyer during circuit discharge, the foil is modeled as an infinitely thin plate, made from a group of straight elementary conductors all carrying the same current density $J = I/w$ across their width. The coordinate system and orientation of the foil and flyer are shown in Fig. 3. The magnetic field (B_x) generated at point (x_p, z_p) by an elementary conductor situated a distance x from the origin is

$$\frac{dB_x}{dx} = \frac{d}{dx}\left(\frac{\mu_0 J}{2\pi r(x)}\right)$$

where

$$r(x) = \sqrt{(x_p - x)^2 + z_p^2}. \tag{9}$$

By integrating the magnetic fields produced by all elementary conductors, the components of the total magnetic flux density produced in the foil are given by

$$B_x(x_p, z_p) = \frac{\mu_0 I}{2\pi w_{\mathrm{foil}}}\left[\tan^{-1}\left(\frac{x_p - w_{\mathrm{foil}}}{z_p}\right) - \tan^{-1}\left(\frac{x_p}{z_p}\right)\right]. \tag{10}$$

In this model, the magnetic field is approximated as being directly above the origin at all times, thus $x_p = 0$. The resulting perpendicular magnetic force F_z to B_x is then simplified to

$$F_z = \frac{(2B_x)^2}{2\mu_0} l_{\mathrm{foil}} w_{\mathrm{foil}}. \tag{11}$$

In a typical electric gun model, the system dynamics are then calculated by adding the foil and flyer mass and determining the system momentum change. The resultant velocity of the foil and flyer are then used to update the foil's position. However, this does not account for the time for pressure information to be passed from the foil to the flyer. This approximation is valid for thin foils and flyers, as the timescales over which information propagation occurs can be assumed to be small when compared to the total flight time. However, the time necessary to communicate a change in velocity in the foil becomes significant where the foil or flyer is thick. This is particularly critical during launch, as the flyer is unable to move off until the first pressure wave has reached its leading surface.

To approximate the 1-D delays in communication of pressure information in 0-D, the foil and flyer are simplified in space to key locations along the z-axis. The model tracks three positions; the rear of the foil, interface between the foil and flyer, and the front of the flyer, visualized in Fig. 3. Prior to launch, the velocity at the rear (v_{zr}) can be found using the total force driving the foil. This velocity state is then assumed to sweep through the foil in the z-direction at the relevant speed of sound, leading to an interface velocity (v_{zi}) found through

$$v_{zi}(t) = v_{zr}\left(t - \frac{h_{\mathrm{foil}}(t)}{c_{s,\mathrm{foil}}}\right) \tag{12}$$

where $c_{s,\mathrm{foil}}$ is the ambient speed of sound in the foil and $h_{\mathrm{foil}}(t)$ is the updated foil thickness. As it lacks an EoS in the flyer material, the model assumes the speed of sound in all materials to be constant, preventing the model from realizing the effects of supersonic shock waves transiting through the flyer. This is an issue, as the foil typically accelerates to velocities higher than the flyer sound speed within hundreds of nanoseconds, causing the interface position to overrun the flyer front in the model. To avoid this, the model updates the front velocity using either the speed of sound in the flyer or the interface velocity to approximate shock behavior that may occur in the flyer using

$$v_{zf}(t) = \begin{cases} v_{zr}\left(t - \left(\dfrac{h_{\mathrm{foil}}(t)}{c_{s,\mathrm{foil}}} + \dfrac{h_{\mathrm{flyer}}(t)}{c_{s,\mathrm{flyer}}}\right)\right), & v_{zi}(t) \le c_{s,\mathrm{flyer}} \\ v_{zr}\left(t - \left(\dfrac{h_{\mathrm{foil}}(t)}{c_{s,\mathrm{foil}}} + \dfrac{h_{\mathrm{flyer}}(t)}{v_{zi}(t)}\right)\right), & v_{zi}(t) > c_{s,\mathrm{flyer}} \end{cases} \tag{13}$$

where $c_{s,\mathrm{flyer}}$ is the speed of sound in the flyer, and $h_{\mathrm{flyer}}(t)$ is the updated flyer thickness. The foil and flyer thicknesses are recalculated at the beginning of each timestep using the positions derived from the three location velocities at each timestep. This allows the model to capture the effect of compression and expansion in the foil and flyer on their dynamics.

C. Pressure Calculation in the Exploding Foil

The maximum pressure and temperature (T) in the foil can be calculated directly using (7) and (11) to find the ohmic heating and the EM force when current I passes through the foil. The two most significant components of pressure in the foil will be those due to the EM force (F_z) and the thermal pressure (P_T). The EM pressure ($P_{B,\max}$) is found using the maximum magnetic field strength (B, max)

$$B_{\max} = \frac{\mu_0 I}{2w} \tag{14a}$$

$$P_{B,\max} = \frac{B_{\max}^2}{2\mu_0}. \tag{14b}$$

In this model, the temperature change (ΔT_B) in the foil due to $P_{B,\max}$ is approximated using the ideal gas EoS

$$\Delta T_B = \frac{P_{B,\max} V(t)}{N k_B} \tag{15}$$

where $V(t)$ is the updated foil volume at that timestep based on $h_{\text{foil}}(t)$, N is the number of molecules and k_B is the Boltzmann's constant. Previous electric gun models have found this simple EoS to give good approximations of the foil behavior, as the foil vaporizes so early in operation [3]. The rise in temperature due to ohmic heating Q_h is then added to T_B to find the total $T(t)$. The change in total temperature ΔT in each time step is then used to find the change in the volume in the foil, with the thermal pressure P_T found using

$$P_T = \frac{n R_0 T(t)}{V(t)}. \tag{16}$$

The model presented allows P_T to contribute to the system dynamics such that

$$\frac{\partial p}{\partial t} = -\frac{P_T}{w_{\text{flyer}} l_{\text{flyer}}} + F_z \tag{17}$$

where p is the combined foil and flyer momentum. Thus, when P_T is expansive it will lead to an increase in the system momentum.

Prior to launch, the foil is confined below the flyer and builds in thermal pressure, unable to expand freely whilst confined between the flyer and the insulation below, which the model assumes to act as a rigid surface. However, after the foil and flyer move away from the origin, the expansion behavior becomes complex as compressive magnetic pressures and expansive thermal pressures influence different regions of the foil. To simplify this behavior in the 0-D model, the volume of the foil is assumed to expand until the front of the flyer moves. After this point, the foil will only expand further if the thermal pressure becomes higher than the magnetic pressure.

D. Pressure Approximation at the Flyer Interface

Unlike the foil, the model has no direct method for calculating the pressure in the insulating flyer as it lacks an EoS. To get around this, the model utilizes three assumptions to estimate the pressure at the foil-flyer interface based on the maximum pressure ($P_{\max}$) in the foil and the position of this maximum ($z_{P_{\max}}$). First, at early times in flight it is assumed there is a single pressure maximum in the foil, which decreases linearly to the pressure at the front of the flyer (P_{z_f}). Second, the pressure is assumed to be continuous across the foil-flyer interface. As a result, the gradient of the pressure can be found using

$$\frac{dP}{dz} = \frac{P_{zf} - P_{\max}}{z_i - z_{P_{\max}} + h_{\text{flyer}}}. \tag{18}$$

Finally, when launch occurs in a vacuum, the model assumes P_f to be zero. Hence the pressure at the interface P_{z_i} is simply calculated using

$$P_{zi} = P_{\max} + \frac{dP}{dz}\left(z_i - z_{P_{\max}}\right). \tag{19}$$

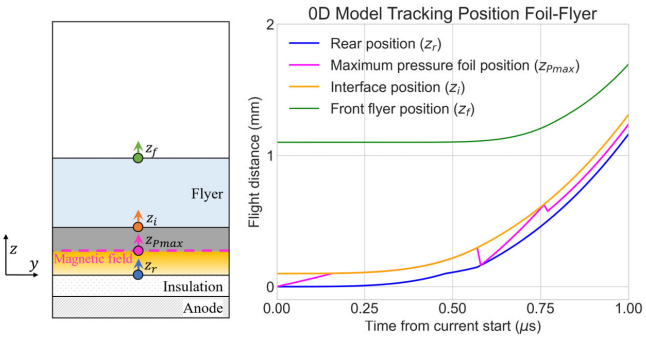

Fig. 4. Four positions tracked by the model, alongside an example of their temporal evolution for the launch of a 0.1 mm thick foil and 1.0 mm thick flyer. The 0-D model approximates the complex dynamic movement of the foil, flyer, and position of maximum pressure in the foil by simplifying the system to four positions along the z-axis, allowing the model to calculate a more accurate interface pressure P_{zi} using 20 without the need for 1-D simulation.

The gradient of the pressure is illustrated in Fig. 3. It can be understood qualitatively using this diagram that for the same $P_{\max}$ and relative z_{Pmax} in the foil, reducing the foil thickness or increasing the flyer thickness will increase the pressure at the flyer interface. These positions are recalculated for each timestep such that the pressure gradient in the model takes into account the changing foil and flyer thickness with regards to the moving position of maximum pressure in the foil, as illustrated in Fig. 4.

The question remains of how to predict the position of the maximum pressure $z_{P_{\max}}$. At early times, the model assumes this will be the same as the position of the magnetic field maximum in the foil. This position can be deduced by understanding the thermodynamic phenomena driving state change in the foil. Initially, the current flows through the foil at the skin depth, generating a magnetic field within the metal. If the magnetic field is strong enough, the EM pressure causes the metal influenced by the field to melt. On melting, the resistivity in the metal increases, allowing the magnetic field to diffuse through the foil, melting the metal it encounters. Lemke et al. [15] referred to these two fronts as the magnetic diffusion front and the melt front and found the speed which this melt front will move through the metal is proportional to the magnetic field strength in the metal plate. Using an MHD hydrocode to simulate a number of experiments with input conditions from the Z accelerator, Lemke found the velocity of the melt line (v_m) in aluminum to be

$$v_m = 0.00127B + 0.596 \tag{20}$$

where B refers in this model to the maximum magnetic field strength in tesla and v_m mm/μs [15]. The model therefore assumes $z_{P_{\max}}$ can initially be calculated using the melt line position, illustrated in Fig. 4, completing the equation for the pressure gradient allowing P_i to be derived.

As the foil and flyer begin to move off, heated metal at the rear of the foil will expand to occupy the space left behind it. This forms a low density region of metallic plasma at the foil rear which is highly conductive, heating the material at the rear of the foil again and further increasing its resistance. When

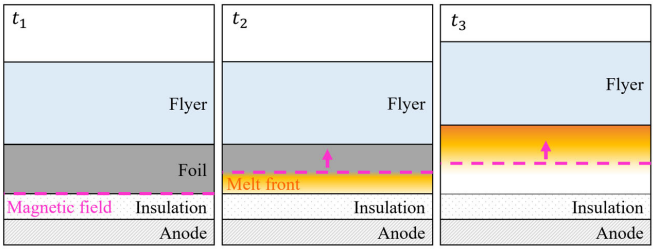

Fig. 5. Position of the magnetic field through the foil starts at the rear of the foil when the current is first discharged (t_1). Ohmic heating and high magnetic field strengths cause the foil to melt, thus the current density accumulates in the lower resistivity region ahead of the "melt line" (t_2). Finally, as the foil and flyer move away from the insulation, low resistivity foil plasma fills the expanding volume, and the current path returns to the rear of the foil. The high current density heats the adjacent foil material and increases its resistivity in this region, thus the magnetic field moves back to the foil rear and begin the process again (t_3).

this occurs, the magnetic field will recede back to this region of higher resistance and cease to follow the material at the melt line. To capture this behavior, the model uses foil temperature and foil positions to identify when the foil temperature exceeds melt and the foil has expanded above its original thickness and moved away from the origin. When this occurs, $z_{P_{\max}}$ is switched from following the melt line to the rear of the foil. The location of the magnetic field maximum with regards to these hydrodynamic effects is illustrated in Fig. 5. Once at the rear again, if the magnetic field continues to be strong enough to heat the foil, it will push forward into the metal once more.

In reality, if the foil is thin $z_{P_{\max}}$ will quickly reach the front of the foil, strongly heating all the metal across the total thickness and causing a drop in density. If this is the case, the magnetic field is able to penetrate the entire foil thickness again as the heating at the rear progresses through the metal. However, in thick foils typically the melt line is still traveling through the foil when the flyer launches and the magnetic field returns to the foil rear. The material that has not interacted with the magnetic field will maintain higher density, and be more difficult for the magnetic field to penetrate on its second oscillation through the foil. To account for this, after moving $z_{P_{\max}}$ to the rear, the model releases it to travel once more at v_m through the foil, but fixes the maximum position the magnetic field can reach on the second excursion to be the same as it reached on the first.

Thermal pressures will also act on the insulating flyer alongside the magnetic pressures. As this model represents the foil as a 0-D object with a maximum temperature assigned to it, it has no knowledge of the temperature distribution throughout the foil. However, the maximum temperature will be the result of both P_b and Q_h, so it is assumed the thermal pressure position to be similar to P_{Bmax}. Hence, the model assumes $P_{\max} = P_{\mathrm{Bmax}} + P_T$ when calculating P_{z_i} when the foil is expanding. Otherwise, the maximum pressure is set as $P_{\max} = P_{\mathrm{Bmax}}$.

III. 0-D Model: Verification Testing Against MHD Hydrocode

The 0-D model presented in the previous section utilizes both EM effects and hydrodynamic behavior in the foil to calculate the flyer dynamics and state. This novel approach of calculating the pressure at the flyer interface using the position of the maximum pressure in the foil and varying foil and flyer thickness requires verification. If the model presented is to be used for design optimization in lieu of a more complex MHD hydrocode, it must produce similar trends and results as the hydrocode in a parameter space of interest.

The hydrocode selected for this task was Code 𝔹, referred to simply as 𝔹 [16]. 𝔹 is an in-house 3-D Eulerian MHD hydrocode developed by First Light Fusion, with volume of fluid interface tracking, utilizing a Lagrangian-remap hydrodynamics scheme, generic plasma EoS and transport coefficients. 𝔹 uses the Frankfurt EoS (FEOS), a semi-analytical tabulated EoS based on the well-known QEOS model [17]. The FEOS was created for high energy density matter regimes. Its ability to better capture liquid–vapor two-phase region using an iterative Maxwell construction scheme makes it suitable for modeling the complex state change in the foil during electric gun launch and flight. 𝔹 has been validated for EM launch on a number of pulsed power loading platforms, and has undergone verification against similar codes such as Gorgon, the Eulerian resistive MHD code developed by Chittenden et al. [18] at Imperial College London.

TABLE I
Machine Parameters for Pulsed Power Capacitor Bank M3

Machine Parameters	Value	[units]
Charge voltage	140	[kV]
Capacitance	124.8	[μF]
Fixed resistance	0.1	[$\mu\Omega$]
Fixed inductance	12.5	[μH]

A. Method: Simulation Configuration and Capacitor Bank

𝔹 has been used extensively to model EM projectile launch on pulsed power platform M3, a 2.5-MJ, 200-kV pulsed power machine at First Light Fusion's onsite facilities [19]. M3 offers a significant research opportunity in the electric gun field, as it would be the highest energy capacitor bank used to power an electric gun in open literature, with a long rise time of around 2 μs. However, previous attempts to experimentally optimize an electric gun for M3 led to flyer failure prior to impact. The flyer failure occurred largely in the early stages of launch, prior to flyer movement. The failure was characterized by high velocity foil plasma breaking through the flyer, indicating a loss of flyer integrity. The load design for these experiments is shown in Fig. 6. This disassembly of the flyer on launch is reflected throughout literature on electric guns [20]. The verification of the model presented focuses on electric gun loads on M3, as the machine is known to induce destructive conditions in flyers. If the model is able to accurately capture these states, it can therefore be used to design a set-up which avoids them. The details of M3 machine parameters used in this work are listed in Table I.

The verification tests presented include a detailed comparison of an individual electric gun case in the model and 𝔹. The detailed comparison was used to evaluate how the accuracy of different variables impacted the final the flyer

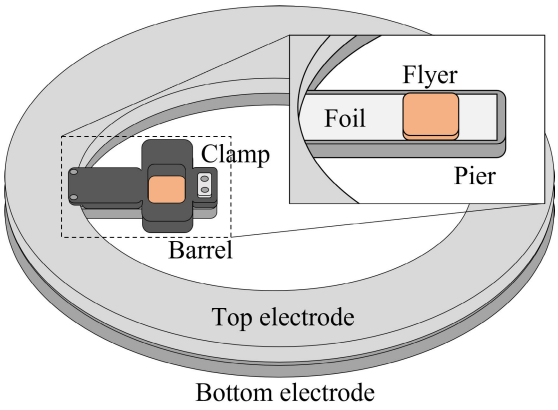

Fig. 6. Simplified diagram showing the electric gun load set-up on M3. The close up shows the flyer atop the foil over the pier, with the barrel hidden from view. The current passes from the pier on the bottom electrode through the foil to the top electrode.

TABLE II
MATERIAL SPECIFIC VALUES FOR ALUMINUM AND PMMA USED IN 0-D MODEL RESULTS [12]

Constant	PMMA	Aluminium	[Units]
Density	1170	2700	$\mathrm{kg\,m^{-3}}$
Sound speed	2757	6320	$\mathrm{m\,s^{-1}}$
Atomic weight (u)	-	26.98	
Melt temperature	-	933.3	K
Boiling temperature	-	2740	K
Specific heat	-	0.9	$\mathrm{kJ\,kg^{-1}}$
Specific heat vapor	-	0.459446	$\mathrm{kJ\,kg^{-1}}$
Enthalpy of fusion	-	396	$\mathrm{kJ\,kg^{-1}}$
Enthalpy of vaporisation	-	11370	$\mathrm{kJ\,kg^{-1}}$

TABLE III
MATERIAL SPECIFIC VALUES FOR ALUMINIUM CONDUCTIVITY MODEL [12]

Constant	Value	[Units]
C1	-5.35×10^{-5}	[mΩ cm]
C2	0.233	
C3	1.21	
C4	0.638	
C5	1.5	
C6	0.012	
C7	3.8×10^{-3}	
C8	18.5	
C9	5.96	
C10	0.44	
C11	3.58×10^{-2}	
C12	3.05	
k	0.878	
L_f	0.107	[Mbar $\mathrm{cm^3/mol}$]
T_{m0}	0.0804	[eV]
Gruneisen coefficent	2.13	

pressure calculation. In addition, a wide-scale parameter scan was performed in both the model and 𝔹 to understand the extent of the model's reliability and probe the validity of the assumptions made in the algorithm. The values used in the model in these cases are included in Tables II and III.

B. Results: Detailed Testcase

The detailed testcase presented was selected to demonstrate the typical launch behavior in an electric gun that the model simulates. It is a 24 × 24 × 0.2 mm aluminum foil driving a 24 × 24 × 1.0 mm PMMA flyer using M3 as the pulsed power driver. The results from the model are presented alongside those from 𝔹 to provide a direct comparison. The pressure in the flyer is a function of the foil state and dynamics. Therefore, the model must correctly estimate the magnitude and temporal features of key variables upstream in the algorithm.

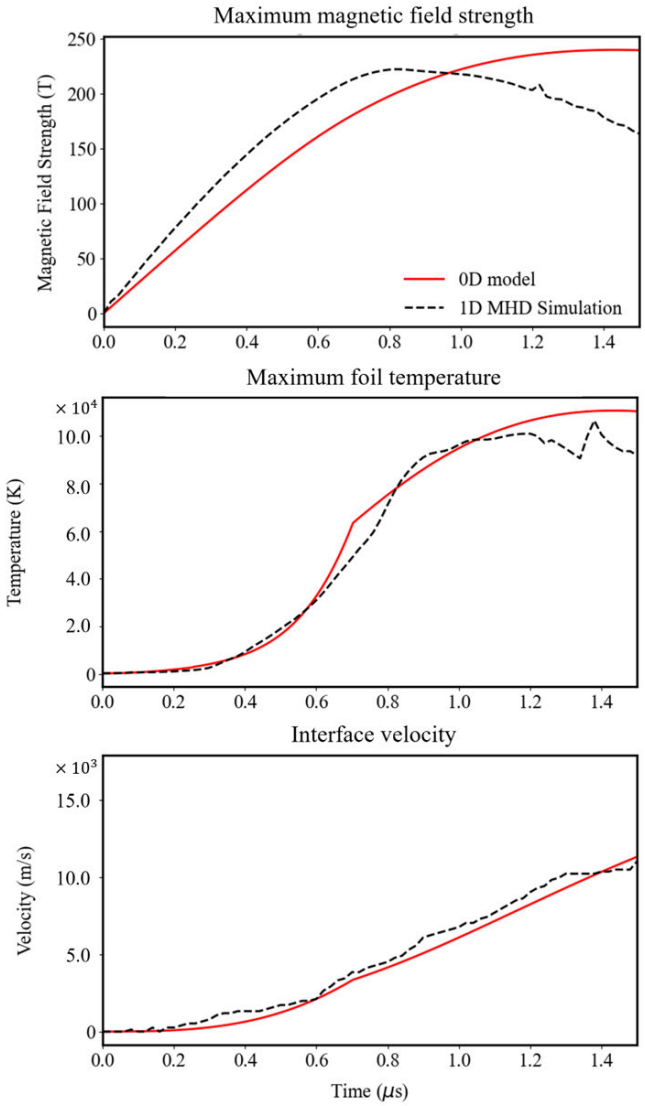

Fig. 7. Plots showing the results from the 0-D model and the 1-D simulation in 𝔹. Despite the differences in the magnetic field strength, the foil temperature and interface velocity predicted by the model are similar to those calculated by 𝔹.

The magnetic field strength and foil temperature drive a number of key calculations and ultimately determine the change in momentum in the system. Fig. 7 demonstrates the magnetic field strength and maximum foil temperature are comparable to results from the 1-D simulation in 𝔹, giving rise to a close match in the velocity profile of the interface position v_{zi}.

The three variables presented in Fig. 7 are then used to calculate the position of the maximum pressure in the foil relative to the flyer interface. The model finds good agreement

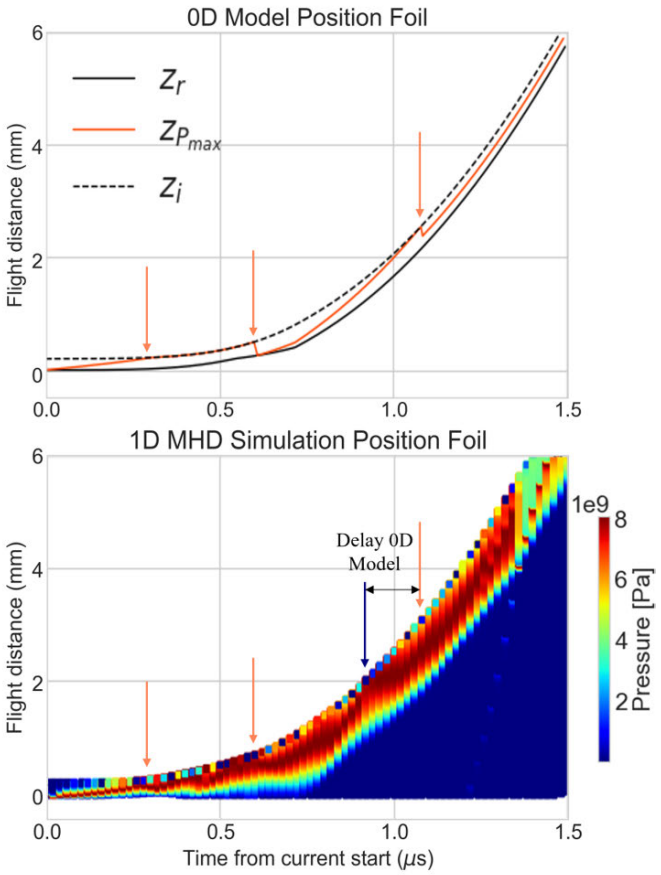

Fig. 8. Comparison of the positions of the rear position (z_r), the interface position (z_i) and the position of maximum pressure (z_{Pmax}) in the 0-D model and 𝔹 over time. At each time step, the position of the foil is plotted, with the 1-D foil material in 𝔹 colored by pressure to highlight the maximum pressure and rear position. z_{Pmax} reaches the interface at 0.35 μs and falls back to the rear surface at 0.6 μs in both the model and the 𝔹 simulation, however, the second excursion arrives at the interface 0.2 μs later in the 0-D model (marked by the orange arrow in the 0-D model and the blue arrow in 𝔹).

with 𝔹 on the position of maximum pressure within the foil during the first excursion though tends to be slightly delayed during the second. For the case shown in Fig. 8, the position of maximum pressure arrived at the foil-flyer interface around 0.2 μs later than in the 1-D 𝔹 simulation. Otherwise, the position of the interface and rear of the foil are in the model match 𝔹 well, showing that it is able to capture compression and expansion behavior in the foil at similar times to 𝔹 despite being 0-D.

The impact of the delay within the foil shown in Fig. 8 on the temporal evolution of the pressure generated in the flyer is apparent in Fig. 9, as the second pressure peak is delayed again by 0.2 μs, whereas the magnitude and temporal evolution of the first pressure peak produced by the model matched 𝔹 very closely. These results suggest the model becomes less accurate at predicting the maximum pressure in the flyer at later times in flight. The error in the calculation of magnetic field strength qualitatively observed in Fig. 7 can be seen in the estimated pressure at the flyer interface in Fig. 9.

These results indicate the pressure in the flyer is most strongly dependent on the position and magnitude of the maximum pressure in the foil with regards to the foil-flyer

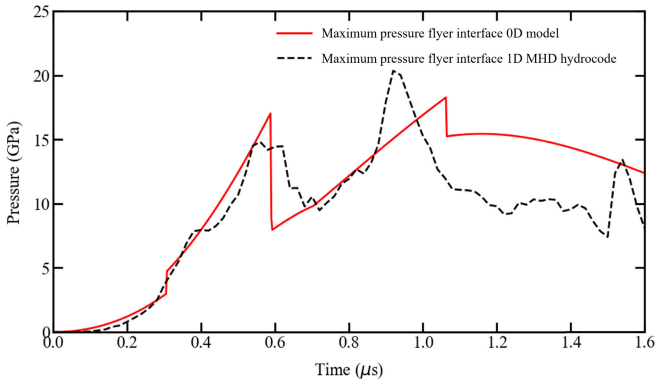

Fig. 9. Comparison between the maximum flyer pressure in the 0-D model and 𝔹. The pressures predicted by the model matches 𝔹 more closely at earlier times in flight, though remain within a factor of 1.5 of the pressures in 𝔹.

interface. In the next section, the 0-D model is exercised over a wide range of initial conditions to further demonstrate its ability to capture salient behaviors in the electric gun launch mechanism.

C. Results: Extended Parameter Scan

To be able to use the 0-D model for wide scale investigation of the electric gun parameter space, the limits of its accuracy must be understood. To achieve this, a large sample of simulations were run in 1-D in 𝔹 and in the 0-D model, across a range of aluminum foil thicknesses, PMMA flyer thicknesses and current densities. The maximum pressure was extracted for each geometry on flyer launch, which was chosen to be the moment the front of the flyer moved in either code. This was a rigorous test of the 0-D model as the value of the pressure on launch relies on both the pressure profile and launch time. The results of this parameter scan therefore assess how well the 0-D model approximates EoS and spatial effects in 1-D MHD simulations.

The 0-D model captured overall trends in how the maximum flyer pressure on launch changed across all three parameters tested. Fig. 10 shows the highest flyer pressure on launch occurred in the electric gun load with the smallest surface area, thinnest foil, and thickest flyer. The pressures in the flyers on launch reduce by roughly the same factor of increase in the surface area in both the model and 𝔹. Second, both codes predicted increasing the flyer thickness led to a greater increase in the flyer pressure than decreasing the foil thickness. Third, both models found the flyer pressure rapidly increased in thick flyers when the foil thickness dropped below around 0.5 mm thickness. This suggests the spike in pressure in electric gun loads with thin foils and thick flyers in this region is due to building thermal pressures in the foil before the flyer moves off. Launch is delayed using thicker flyers, as the initial pressure wave must travel further to reach the front of the flyer, causing the thermal pressure to increase in the trapped vaporized foil until its volume is able to expand as the flyer moves off. It is the 0-D model's ability to track the flyer interface and front as separate points with different velocities that enables it to capture this effect.

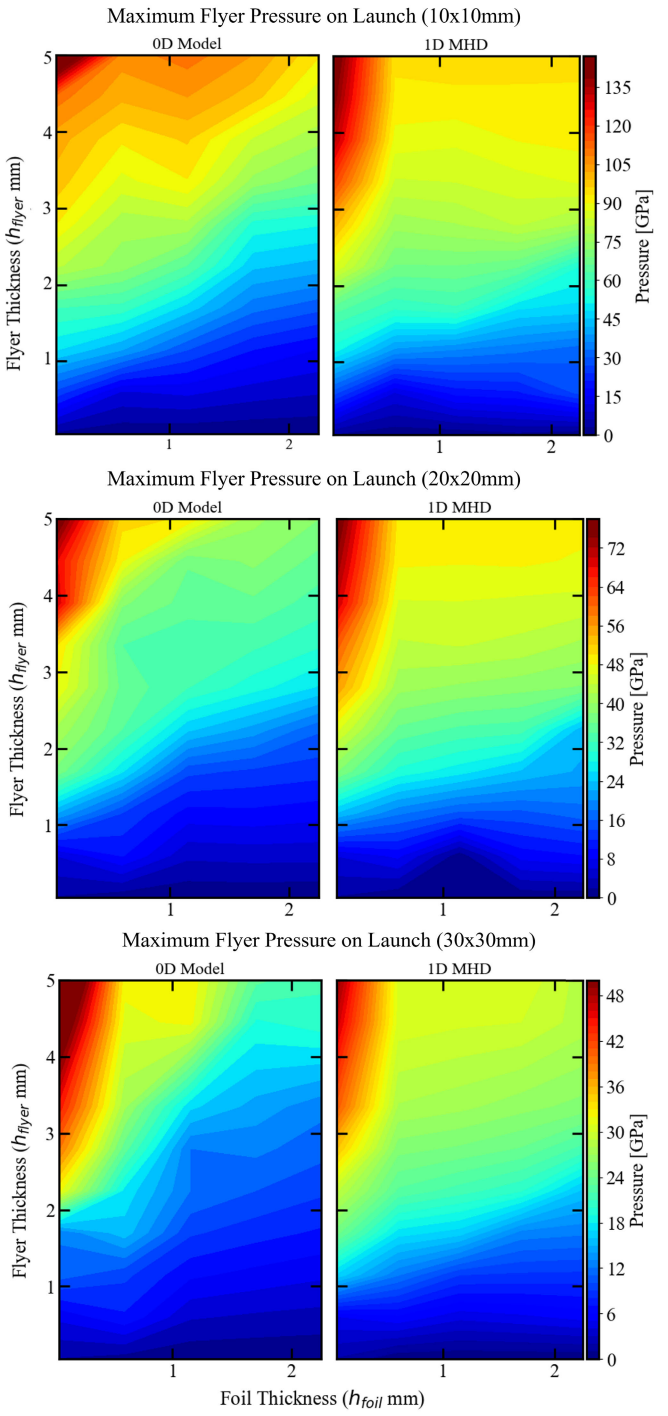

Fig. 10. Heatmap of maximum flyer pressure on launch across a range of foil and flyer thicknesses, with varying surface area.

The difference in the maximum flyer pressure on launch predicted by the 0-D model and B2 is compared in Fig. 11. The model closely replicates 𝔹 where the pressure contours overlap. Over all three current densities, the pressure estimation of the 0-D model is best when the foil is thin. Across all three surface areas, flyers driven by thin foils show good agreement with 𝔹 across the range of flyer thicknesses. By analyzing the pressure contours across the parameter space investigated, it can be deduced the maximum discrepancy between the codes is roughly a factor of 2.5.

Results from the parameter scan demonstrate the model correctly identifies nonlinear trends in the maximum pressure on launch across a range of current densities. It is able to predict the spike in the flyer pressures prior to launch in electric gun loads with thin foil and flyers above around 3.0 mm. The model is able to replicate these more complex trends due to the novel features implemented which allow it to track the flyer positions and pressure gradient. The 0-D model replicates the 1-D MHD simulations best for setups with thin foils. Discrepancy with 𝔹 increases to a maximum in geometries with the highest surface area and thickest foil.

D. Results: Validation Testcases

Modeling the electric gun in 0-D space.

E. Discussion: Assessment of Assumptions in the 0-D Model Across Parameter Space

The results shown in the previous section present data from both 1-D MHD simulations in hydrocode 𝔹 alongside those from the 0-D model. The detailed testcase illustrated the accuracy of key variables in the model algorithm, whilst the parameter scan provided a broader picture of the model's ability to match the 1-D MHD simulations across a range of electric gun geometries. The results also highlighted the time periods across which the 0-D model most closely matched 𝔹. These are due to some of the approximations made in the algorithm to simplify the problem.

First, the analysis of the detailed test case demonstrated the model is capable of capturing the temporal variations in the maximum pressure in the flyer throughout flight. Fig. 9 demonstrated the flyer experiences two distinct pressure maxima, which align with the movement of the position of maximum pressure within the foil shown in Fig. 8. This supports the 0-D model's assumptions that the maximum pressure in the foil will be located in the region of lowest resistivity, which in turn moves according to the melt front and position of the foil. Additionally, the accuracy in the flyer pressure predictions suggest the treatment of the foil-flyer interface as a continuous interface, across which the pressure gradient varies linearly, is also valid. The detailed testcase illustrated both these elements of the model match 𝔹 more closely earlier in the current rise time. This is to be expected, as the equation for the melt line velocity developed by Lemke et al. [15] was derived for the first current density excursion through the foil, not the second. Complex phenomena such as secondary shocks in the exploding foil plasma, which the 0-D model cannot capture, also contribute to late time variation in the pressure in the flyer. However, even at these late times the 0-D model continues to match 𝔹's maximum pressure within a factor of around 1.5, suggesting the most important elements of the physics are still being captured.

The parameter scan results indicated the model is able to replicate trends in flyer pressure on launch across the parameter space investigated. The model most closely predicted the magnitudes of the pressure for geometries with thin foils, across the range of flyer thicknesses tested. This supports the conclusions drawn from the detailed testcase that the model is

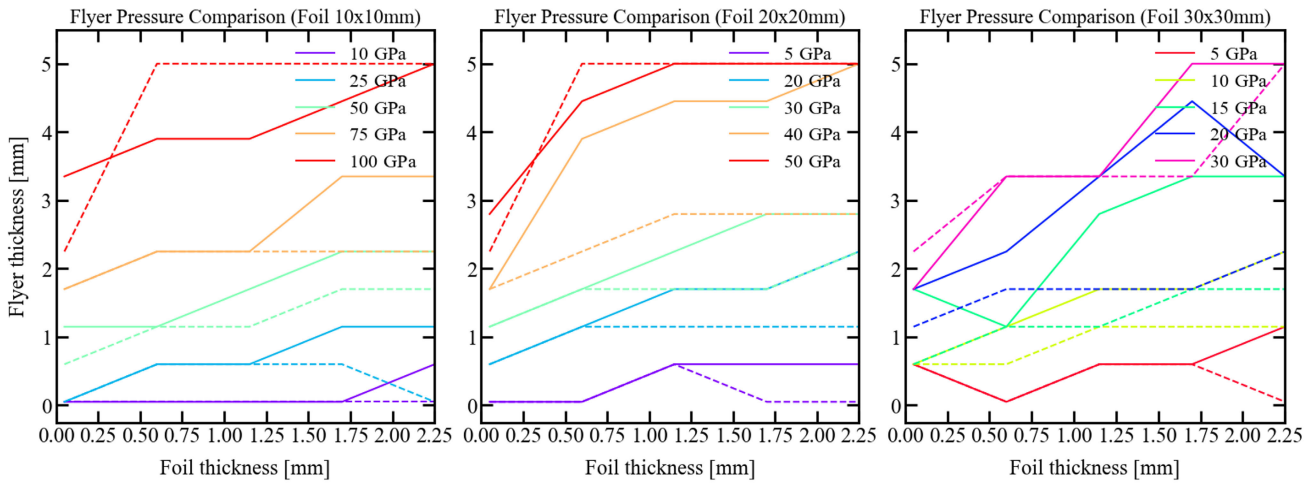

Fig. 11. Contour plots comparing the maximum flyer pressure on launch for varying foil and flyer thicknesses for different foil surface areas in 1-D MHD 𝔹 simulations *(dotted line)* and the 0-D model *(solid line)*. The contours across all foil surface areas show the model underestimates the pressure in thicker flyers, with the error increasing to a factor of around 2.5 in the loads with surface area of 30 × 30 mm and thick foils.

more accurate at earlier times, as launch occurs more rapidly in cases with thin foils. The scan showed the flyer pressure is highest in cases with thin foils and thick flyers, therefore, these load geometries are likely to be most at risk of flyer failure. This indicates the model matches 𝔹 best in the most critical regions of the parameter space, making it a powerful design tool for electric gun set-ups accelerating thick flyers.

Overall, the results from the verification study suggest the 0-D model is reliable over a wide region of the geometric parameter space, but importantly, is most accurate for critical time periods and load parameters. Experimental results have implied thick flyers are most likely to fail at early flight times, which is when the approximations made by the model are most valid [20]. This implies the physics chosen to be included in the algorithm is appropriate for the task of optimizing an electric gun set-up for a range of flyer thicknesses and geometries.

IV. Conclusion

In this work, the model presented is capable of predicting not only the dynamics of a flyer launched by an electric gun, but also the maximum pressure states in the flyer throughout flight. The results from the model were verified against 1-D MHD simulations in the in-house hydrocode Code 𝔹. Comparison between the codes using both a detailed testcase and wide ranging parameter scan revealed the physics and assumptions governing the model were most accurate at early current rise times, in flyers launched by thin foils. It was concluded as follows.

1) The flyer pressure can be calculated in the model without need for an EoS, based on previous understanding of the movement of the melt line in the foil. By approximating the position of maximum current density in the foil, thereby locating the position of the maximum pressure for calculation of a pressure gradient across the foil-flyer interface, the model is able to reduce the required computational resource.
2) Both the magnetic field strength and the position of the foil were found to determine the position of the maximum pressure in the foil. The thermal pressure in the foil was only found to act on the flyer when the foil was expanding, whereas the magnetic pressure in the foil contributed to the pressure gradient at all times.
3) The verification parameter scan showed the pressure in the flyer on launch was most sensitive to flyer thickness in loads with thin foils. Before launch the foil volume is constrained, driving higher thermal pressures in the foil until it is able to move off as the current continues to rise. As thicker flyers delay launch, the building pressures in the foil vapor drive a rapid spike in maximum pressure at the foil-flyer interface.
4) The model presented is most accurate at earlier times in flight, as this is when the approximations made in the algorithm such as constant sound speed and pressure location based on the melt line velocity are most accurate.

Validation performed comparing the model against experimental results collected from a range of electric gun loads will be presented in a forthcoming paper [3], [6], [21]. This dataset will include pulsed power devices with differing rise times and energetic capacities to understand the effect of the current profile on the model behavior. In future work, the model will be used to redesign an electric gun load for the 2.5 MJ capacitor bank M3, based on the maximum flyer pressure states calculated for a successful electric gun shot on another smaller pulsed power machine, CEPAGE [22]. Using the states in the flyer on CEPAGE as a guide, the geometries of the foil and flyer which generate this pressure in a flyer on M3 will be determined. The design will then be experimentally tested on M3 in order to investigate the effect of long rise times on flyer state late in flight.

Acknowledgment

The authors gratefully acknowledge the support provided by First Light Fusion, Yarnton, U.K., both in terms of sponsorship of M. D. Fitzgerald's D.Phil., and through skills and expertise of the numerical team.

REFERENCES

[1] R. Weingart et al., "Electric gun: A new tool for ultrahigh-pressure research," California Univ., Lawrence Livermore Lab., Livermore, CA, USA, Tech. Rep. UCRL-52752 TRN: 79-015919, 1979.

[2] J. E. Osher, H. H. Chau, G. R. Gathers, R. S. Lee, and R. C. Weingart, "Application of a 100-kV electric gun for hypervelocity impact studies," *Int. J. Impact Eng.*, vol. 5, nos. 1–4, pp. 501–507, Jan. 1987.

[3] J. E. Osher et al., "Operating characteristics and modeling of the LLNL 100-kV electric gun," *IEEE Trans. Plasma Sci.*, vol. 17, no. 3, pp. 392–402, Jun. 1989.

[4] W. Guiji et al., "Speed test of small size flyer of explosive foil detonator," Ph.D. dissertation, China Acad. Eng. Phys. (CAEP), Sichuan, China, 2008.

[5] G. Wang et al., "The techniques of metallic foil electrically exploding driving hypervelocity flyer to more than 10 km/s for shock wave physics experiments," *Rev. Sci. Instrum.*, vol. 82, no. 9, Sep. 2011, Art. no. 095105.

[6] Z. Song, J. Mo, J. Zhao, F. Tan, and H. Yuan, "Study on launching technique of a 98 kJ electric gun for hypervelocity impact experiments," *Int. J. Impact Eng.*, vol. 122, pp. 419–430, Dec. 2018.

[7] R. Varesh, "Electric detonators: EBW and EFI," *Propellants, Explosives, Pyrotechnics*, vol. 21, no. 3, pp. 150–154, Jun. 1996.

[8] R. W. Lemke et al., "Characterization of magnetically accelerated flyer plates," *Phys. Plasmas*, vol. 10, no. 4, pp. 1092–1099, Apr. 2003.

[9] R. S. Lee, J. E. Osher, H. H. Chau, G. Pomykal, and R. D. Speer, "1 MJ electric gun facility at LLNL," *IEEE Trans. Magn.*, vol. 29, no. 1, pp. 457–460, Jan. 1993.

[10] R. Weingart, R. Lee, R. Jackson, and N. Parker, "Acceleration of thin flyers by exploding metal foils: Application to initiation studies. [PETN, TATB, PBX-7404, NM]," California Univ., Lawrence Livermore Lab., Livermore, CA, USA, Tech. Rep. UCRL-77610; CONF-760805-10, 1976.

[11] I. R. Lindemuth, J. H. Brownell, A. E. Greene, G. H. Nickel, T. A. Oliphant, and D. L. Weiss, "A computational model of exploding metallic fuses for multimegajoule switching," *J. Appl. Phys.*, vol. 57, no. 9, pp. 4447–4460, May 1985.

[12] G. Wang, J. Zhao, B. Luo, and J. Jiang, *Magnetohydrodynamics of Metallic Foil Electrical Explosion and Magnetically Driven Quasi-Isentropic Compression*. Rijeka, Croatia: InTech, 2011.

[13] B. M. Novac, K. Omar, N. Graneau, I. R. Smith, and M. Sinclair, "Numerical modelling of a flyer plate electromagnetic accelerator," *IEEE Trans. Plasma Sci.*, vol. 40, no. 10, pp. 2300–2311, Oct. 2012.

[14] T. J. Burgess, "Electrical resistivity model of metals," Pulsed Power Theory Div., Sandia Nat. Labs., Albuquerque, NM, USA, Tech. Rep. SAND-86-1093C; CONF860703-28; ON: DE86014298, 1986.

[15] R. W. Lemke, M. D. Knudson, K. R. Cochrane, M. P. Desjarlais, and J. R. Asay, "On the scaling of the magnetically accelerated flyer plate technique to currents greater than 20 MA," *J. Phys., Conf. Ser.*, vol. 500, no. 15, May 2014, Art. no. 152009, doi: 10.1088/1742-6596/500/15/152009.

[16] J. D. Pecover. (2019). *Demonstration of Numerical Capability at First Light Fusion*. [Online]. Available: https://firstlightfusion.com/science-hub/demonstration-of-numerical-capability-at-first-light-fusion

[17] S. Faik, A. Tauschwitz, and I. Iosilevskiy, "The equation of state package FEOS for high energy density matter," *Comput. Phys. Commun.*, vol. 227, pp. 117–125, Jun. 2018.

[18] J. P. Chittenden, S. V. Lebedev, C. A. Jennings, S. N. Bland, and A. Ciardi, "X-ray generation mechanisms in three-dimensional simulations of wire array Z-pinches," *Plasma Phys. Controlled Fusion*, vol. 46, no. 12B, pp. B457–B476, Dec. 2004.

[19] P. Holligan et al., "An overview of the diagnostic developments for M3, a 2.5 MJ low inductance capacitor discharge machine," in *Proc. APS Division Plasma Phys. Meeting Abstr.*, 2018.

[20] J. Osher, R. Gathers, H. Chau, R. Lee, G. Pomykal, and R. Weingart, "Hypervelocity acceleration and impact experiments with the LLNL electric guns," *Int. J. Impact Eng.*, vol. 10, nos. 1–4, pp. 439–452, Jan. 1990.

[21] B. Luo, J. Mo, C. Xu, X. Chen, and R. Shui, "A 200 kJ electrical gun for hypervelocity launch," *Rev. Sci. Instrum.*, vol. 92, no. 12, Dec. 2021, Art. no. 123905.

[22] A. Lefrançois, P.-Y. Chanal, G. Le Blanc, J. Petit, G. Avrillaud, and M. Delchambre, "High-velocity flyer-plate developments on two high-pulsed-power generators based on a strip-line design (GEPI and CEPAGE)," *IEEE Trans. Plasma Sci.*, vol. 39, no. 1, pp. 288–293, Jan. 2011.

Mila D. Fitzgerald received the M.Eng. degree from the Univesity of Oxford, Oxford, U.K., in 2020, where she is currently pursuing the Ph.D. degree.

She is also a Scientist at the Numerical Physics Team, First Light Fusion, Yarnton, U.K., a private company researching projectile driven inertial confinement fusion. Her research focuses on modeling and experimental design of electromagnetic launch techniques for fusion and extreme state research.

James D. Pecover received the undergraduate degree in physics from the University of Sheffield, Sheffield, U.K., in 2010, and the Ph.D. degree in plasma physics from the Imperial College London, London, U.K., in 2015.

Since 2017, he has been worked at First Light Fusion Ltd., Yarnton, U.K., as a Numerical Physicist. His research interests include simulation of electromagnetic projectile launch, shock physics, and equation of state.

Nik Petrinic is a developer and integrator of experimental, analytical, and numerical methodologies on the border between mathematics, physics, materials science, mechanics of materials, and computer science, aimed at addressing the emergence of new materials and their application in extremely demanding engineering applications. He leads a multidisciplinary research team which investigates hygro/hydro-thermal-pressure-and-rate dependent behavior of materials, systems, and structures at a wide range of length scales and anticipated in-service environmental and loading conditions, in close collaborations with partners in academia, industry, and government agencies.

Daniel E. Eakins is an experimental scientist working at the interface of "extreme" materials science, shock physics, and dynamic measurement science. He conducts research on the ultrafast behavior of materials under extreme loading conditions, using a combination of gas-guns and high-power lasers to study key physical processes from their lattice-level origins to the bulk scale.